The structure, modelling and dynamics of hindered 5,6-diarylacenaphthenes

Wendy Cross,[a] Geoffrey E. Hawkes,[b] Romano T. Kroemer,[b] Klaus R. Liedl,[c] Thomas Loerting,[c] Rima Nasser,[b] Robin G. Pritchard,[a] Melanie Steele,[a] Michael Watkinson[b] and Andrew Whiting*[a]

[a] *Department of Chemistry, UMIST, PO Box 88, Sackville Street, Manchester, UK M60 1QD*
[b] *Department of Chemistry, Queen Mary and Westfield College, Mile End Road, London, UK E1 4NS*
[c] *Institute of General, Inorganic and Theoretical Chemistry, University of Innsbruck, Innrain 52a, A-6020 Innsbruck, Austria*

Received (in Cambridge, UK) 1st November 2000, Accepted 24th January 2001
First published as an Advance Article on the web 16th February 2001

A series of 5,6-diarylacenaphthenes, **2**–**4**, has been investigated using a variety of theoretical and experimental methods. The purpose of the investigation was to gain a thorough understanding of the dynamics of atropisomer interconversion in these molecules. Quantum chemical calculations were performed at different levels, including Hartree–Fock theory, density functional theory (B3LYP), and a semi-empirical method (AM1). Basis sets used ranged from STO-3G to 6-31+G*. The structures of energy minima and transition states for *anti–syn* interconversion were fully optimised. A geometrical comparison of the single-crystal X-ray structures of *syn*-**2b**, *anti*-**2c** and *anti*-**2d** was made with the results from the calculations, and revealed excellent agreement in most cases. Theoretical barriers to rotation were compared with those derived experimentally by NMR spectroscopy. Again excellent correlation between theoretical and experimental values was found. In the transition states a significant deviation from planarity for the acenaphthene moiety was calculated. The transition state structures indicate why bulky substituents, such as Bu^t, in the 3′ and 3″ positions of the *peri*-aryl rings are not able to prevent atropisomer interconversion. The structures provide a good explanation for the trends observed in experimental barriers to rotation.

Introduction

House and co-workers first reported the preparation of 1,8-diarylnaphthalenes, after postulating that 1,8-diaryl rings would be too large to allow interconversion between atropisomers **1a**–**1b**.[1a] Subsequent studies of representative compounds, prepared with *meta*-substituents on the *peri*-diaryl rings, showed that there was a dynamic equilibrium at room temperature between *syn*- and *anti*-atropisomers, with rotational energy barriers in the range of 10–16 kcal mol^{-1}.[1b–e] These surprisingly low energy barriers to rotation had one important consequence: namely chiral C_2-symmetric systems, such as **1b**, are not configurationally stable at room temperature and hence could not be used in asymmetric synthesis and catalysis, in direct contrast to other configurationally stable C_2-symmetric atropisomers, such as 1,1′-bi-2-naphthol.[2] Despite extensive investigation from other groups on the effects that symmetrical[3] and unsymmetrical[4] diaryl ring substituents have on the rotational energy barriers to interconversion between 1,8-diarylnaphthalene atropisomers, the basic problem of the prevention of aryl ring rotation has not been solved.

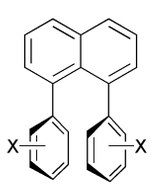

1

a; X groups *syn*
b; X groups *anti*

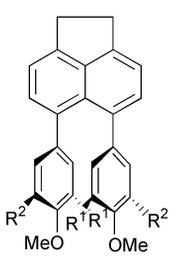

2

a; $R^1 = R^2 = H$
b; $R^1 = Me$, $R^2 = H$
c; $R^1 = Bu^t$, $R^2 = H$
d; $R^1 = Bu^t$, $R^2 = Me$

Recent work in our laboratories has involved the use of 1,8-diarylnaphthalene systems as scaffolds for the construction of bis-manganese complexes[5] and, more recently, the synthesis of potentially chiral, hindered 5,6-diarylacenaphthene systems.[6] These recent studies have concentrated on developing synthetic approaches to structures of the general type **2** and the optimisation of the coupling methods required for the synthesis of such hindered systems.

In order to exploit 1,8-diarylnaphthalenes as potential C_2-symmetric chiral catalysts, one requires a system in which: a) there is a substantial difference in the steric demand between the blocking groups across the ligand framework; b) the differentially sized blocking groups should be as close to the ligand binding functions as possible and preferably directed towards the likely catalytic site; and c) there is complete conformational stability. Systems of the general type **2** appeared to be ideal for application as potential new chiral ligand precursors; structure **2** possesses readily cleavable methyl ethers and the substituents in the positions *ortho* to the methoxy group should be readily adjustable. We therefore undertook the synthesis of the simplest version of **2**, *i.e.* **2a**, with the aim of derivatising the position(s) *ortho* to the methoxy groups. This approach proved to be impossible, due to the proximity of the phenyl rings, and as a result functional groups

DOI: 10.1039/b008788m

R^1 and R^2 had to be introduced into the phenylboronic acid coupling precursors of **2**. By this method, **2b–d** were readily accessed using Suzuki coupling methods; however, it was apparent from attempts to separate the atropisomeric forms of **2b–d** that these structures were not sufficiently stable for application as new chiral ligands.[6] In order to fully understand the exact requirements for atropisomeric stability in systems such as **2**, fundamental structural and dynamic information was required to enable the design and subsequent synthesis of atropisomerically stable versions of **2**.

In recent years, there have been several studies which examined the structure and dynamics of diarylnaphthalene systems. Semi-empirical methods have been used to locate the transition state involved in the rotation process for certain dipyridyl and dipyrimidyl naphthalene systems and calculate rotation barriers.[7] This work is in broad agreement with NMR data, which suggest barriers to rotation of 11–16 kcal mol^{-1}. Cozzi and Siegel have also demonstrated[8] the effect of the relative polarisation of the phenyl rings in diphenylnaphthalene systems, which strongly suggests that substituents *ortho* to the naphthalene and polar π-interactions can have a profound effect upon rotation barriers, resulting in barriers ranging up to 26.2 kcal mol^{-1}. To increase rotation barriers above this level seemingly requires the preparation of highly hindered systems, not necessarily diphenylnaphthalene derived. Thus, highly hindered 1,8-(1,2,3-triazolyl)naphthalene can produce rotation barriers as high as 24 kcal mol^{-1}.[9] It was therefore important for us to determine what influence a stepwise steric build up would have upon the structures **2**, to provide a platform for the rational design of new ligands based upon atropisomerically stable 1,8-diarylnaphthalene or structurally similar systems. In this paper, we report high level theoretical modelling calculations on systems **2** and compare these results to both solid state X-ray crystallography and NMR-derived solution structure and dynamic results.

Methods

Molecular modelling

Throughout this manuscript we will use the STO-3G data as a qualitative guide, and will refer to higher level calculations and experimental data wherever possible. Quantum chemical calculations were carried out on compounds **2b–d**, **3** and **4** using the Gaussian 98 program.[10] Energy profiles for *anti* to *syn* conversion of selected compounds were computed at the AM1[11] and HF/STO-3G[12] levels of theory. These profiles were obtained from relaxed potential energy surface scans, *i.e.* systematic modification of one of the two naphthyl–aryl torsions (defined by atoms 4–5–1′–2′, *vide infra*) from 60 (*anti*-conformation) to 240 (*syn*-conformation) degrees in 10 degree increments and subsequent geometry optimization (with the dihedral angle being constant). For some of the molecules the geometries of stationary points (*anti*-conformation, transition-state, *syn*-conformation) were fully optimized without symmetry constraints at the HF/STO-3G, HF/3-21G,[13] and HF/6-31G*[14] levels of theory. Harmonic vibrational frequencies were computed in order to characterize stationary points (minima and first-order saddle points, the latter having exactly one imaginary frequency). DFT calculations were performed employing the B3LYP functional[15] and a 6-31+G* basis.[14,16] Self-consistent reaction field (SCRF) calculations were carried out at the Hartree–Fock level with the Onsager reaction field model[17] and a 6-31+G* basis. Throughout the paper the theoretical level used for geometry optimisation will be denoted as method/basis set (*e.g.*, HF/6-31G* stands for Hartree–Fock method with a 6-31G* basis set). Single point calculations at a higher level using geometries optimised at a lower level will be denoted as higher level//lower level (*e.g.*, HF/6-31+G*//HF/3-21G).

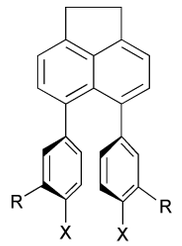

3

a; R = Me, X = H
b; R = Bu^t, X = H
c; R = Bu^t, X = OH
d; R = Me, X = OH

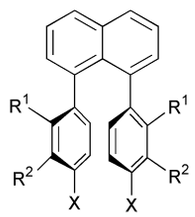

4

a; R^1 = H, R^2 = Me, X = H
b; R^1 = H, R^2 = Bu^t, X = H
c; R^1 = H, R^2 = Bu^t, X = OMe
d; R^1 = Me, R^2 = X = H

Single crystal X-ray diffraction

Crystal structures have been determined for molecules *syn*-**2b**, *anti*-**2c** and *anti*-**2d**.† All X-ray measurements were performed on automated 4-circle diffractometers employing graphite monochromated X-rays. A Nonius MACH3 (Mo Kα, λ 0.71069 Å) was used for *anti*-**2c** and a Rigaku/MSC AFC6S (Cu Kα, λ 1.54178 Å) for *syn*-**2b** and *anti*-**2d**. Unit cell parameters were obtained by least-squares refinement based on the setting angles of 25 reflections (in the θ ranges 11–16° for Mo Kα and 20–36° for Cu Kα). Crystallographic data for the molecules are presented in Table 1. The structures were solved by direct methods using SHELXS97 and refined by full-matrix least-squares using SHELXL97.[18]

NMR Spectroscopy

All ^{1}H NMR spectra were measured at 600 MHz using a Bruker AMX600 spectrometer. Samples were contained in 5 mm o.d. tubes and solutions were made from *ca.* 5 mg compound in 0.5 ml $CDCl_3$ (**2b–d**) or in 0.5 ml of the cryoprotective mixture $(CD_3)_2SO$–D_2O 80 : 20 v/v (**3c**). Attempts to measure qualitative nuclear Overhauser enhancement (NOE) connectivities between protons using the 2-dimensional NOESY experiment were largely unsuccessful due to the very weak correlation (cross) peaks obtained. This was certainly due to motional 'nulling' of the NOE at the observation frequency of 600 MHz, and therefore the ROESY experiment was used, with mixing times in the range 100–300 ms, to explore the NOE and slow chemical exchange effects.[19] For the variable temperature experiments the temperature controller was calibrated against a standard methanol sample, and the reported temperatures are believed to be accurate to ±1 °C. The spectral simulations of the band shapes were performed with a PC using the Bruker software WIN-DYNA.[20]

Results and discussion

Molecular modelling

The *anti* to *syn* conversion energy profiles for selected compounds calculated at the AM1 and HF/STO-3G levels are displayed in Fig. 1. The atomic numbering used in the following discussion is as shown. It is obvious that there is a large difference between the two theoretical levels for the calculated gas phase activation barriers for rotation. Earlier studies on 1,8-dihetarylnaphthalenes[7] have shown that semi-empirical methods tend to underestimate rotational barriers in similar systems. The energy profiles reveal several trends. The change of the *tert*-butyl substituent to the methyl group in the 3′/3″-position has only a minor influence on the energetics of

† CCDC reference numbers 145452, 145453 and 100797. See http://www.rsc.org/suppdata/p2/b0/b008788m/ for crystallographic files in .cif format.

Table 1 Selected crystallographic data for **2b**–**2d**

	syn-**2b**	*anti*-**2c**	*anti*-**2d**
Temperature/K	293	293	293
Crystal size/mm^3	0.30 × 0.25 × 0.10	0.30 × 0.30 × 0.25	0.35 × 0.25 × 0.15
Molecular formula	$C_{28}H_{26}O_2$	$C_{34}H_{38}O_2$	$C_{36}H_{42}O_2$
Crystal system	Triclinic	Monoclinic	Monoclinic
Space group	$P\bar{1}$	$C2/c$	$P21/c$
a/Å	10.547(2)	15.426(11)	14.053(3)
b/Å	11.975(2)	12.426(10)	13.639(4)
c/Å	9.011(3)	15.224(10)	15.490(3)
β/°	92.85(2)	108.59(6)	94.00(2)
α, γ/°	111.51(2), 88.69(2)	—	—
Z	2	4[b]	4
λ/Å	1.54178	0.71069	1.54178
Reflections collected	7038	2548	5035
Independent reflections	3468	2451	4819
Reflections observed[a]	2156	1288	2369
θ range for data collection/°	4–65	2–25	3–65
Restraints (parameters)	(0) 376	(0) 240	(9) 512
R_1 (observed reflections)	0.076	0.052	0.047
wR_2 (all reflections)	0.259	0.163	0.168
Goodness-of-fit on F^2	1.005	0.985	1.025

[a] Criterion for observation: $F^2 > 2\sigma(F^2)$. [b] Each molecule has crystallographic C_2 symmetry. [c] Refinement against F^2.

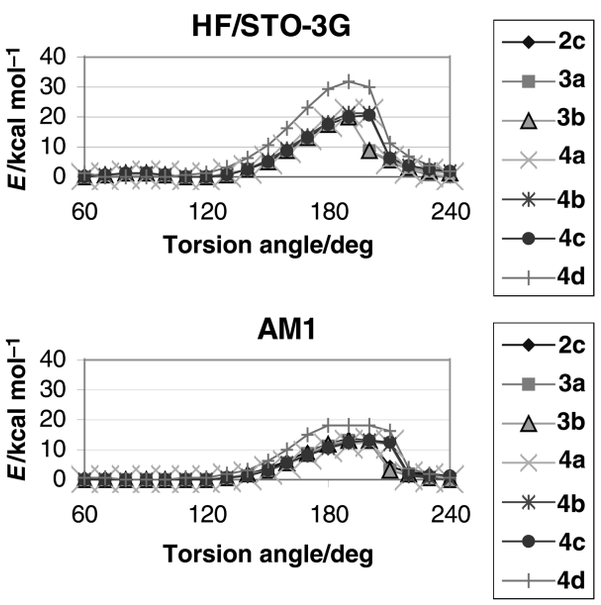

Fig. 1 Energy profiles for *anti* to *syn* conversion in selected compounds, calculated at two levels of theory.

the rotation (*cf.* the pairs **3a/3b** and **4a/4b**). Omission of the "bridge" does not have a pronounced effect on the activation barrier either, but it changes the maximum of the barrier from 190 to 200 degrees along the rotational co-ordinate. The latter can be observed at both levels of theory. A possible interpretation of this phenomenon could be based on the prediction that in the transition state (TS) the planarity of the naphthalene system is distorted (see below). The "bridge" containing two sp^3-hybridized carbons assists in distorting this planarity. Consequently, the TS can be reached at an earlier point along the rotational co-ordinate.

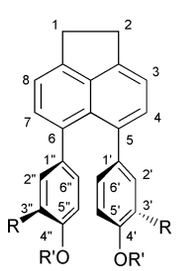

For several molecules the stationary points on the *anti* to *syn* conversion pathway were fully optimized at various levels of theory. The corresponding relative energies are listed in Table 2. The HF/3-21G geometries corresponding to the stationary points of *anti*-**3b** to *syn*-**3b** conversion are displayed in Fig. 2. In both the *syn*- and *anti*-forms the benzene rings are not entirely parallel to each other. The rings are closer to each other at the 1′/1″ carbon, and the angle between the rings' planes is approximately 14 degrees. Animation of the imaginary frequency for **3b**-TS verifies that the transition state corresponds to a rotation about the aryl–naphthyl (4–5–1′–2′) torsion. This rotational motion is accompanied by a flattening motion of the naphthalene ring system. The value for the 4–5–1′–2′ dihedral angle is 186.1 degrees. The structures in Fig. 2 reveal some interesting features, which are common to all the molecules investigated. The geometry of the TS is characterized by a significant non-planarity of the naphthalene ring system. The ring system is distorted in such a way that both aryl rings are found on opposite sides of an idealized plane through the naphthalene carbon atoms. This distortion increases the distance between the two rings, hence reducing steric repulsion in the transition state. The main contribution to the activation barrier for rotation appears to result from the unfavourable steric interaction between an *ortho*-hydrogen (attached to C2′) and the other aryl ring.

The HF/STO-3G energies compare fairly well with experimentally determined barriers for rotation reported by Clough and Roberts.[3a] However, we also performed calculations at higher levels of theory, in order to obtain benchmarks for these molecules for future use. In this context we explored different basis sets as well as different theoretical concepts (*cf.* Table 2). Because of the considerable size of the molecules the higher level calculations were performed only on selected representatives and preferably on the smaller ones.

In general, application of larger basis sets than STO-3G leads to a reduction in the calculated activation barriers at the Hartree–Fock level, and using the 3-21G basis lowers the activation energy by 2–4 kcal mol^{-1}. Larger basis sets (6-31G* and full geometry optimisation of **3a**, or 6-31+G* and single point calculation for the HF/3-21G geometry of **2b**) appear not to reduce this barrier further. For **2b** the activation enthalpy of +17.85 kcal mol^{-1} at the HF/3-21G level is already in excellent agreement with the experimental value of 17.33 kcal mol^{-1} (*vide infra*). Also for **2c** the agreement is markedly improved at this level of theory. In the case of **2d** the activation energy is slightly underestimated at the HF/3-21G* level, but it reflects

Table 2 Relative energies (kcal mol^{-1}) for selected molecules[a]

	2b		**2c**		**2d**		**3a**		**3b**		**3c**	
Method	→TS	→*syn*	→TS	→*syn*	→TS	→*syn*	→TS	→*syn*	→TS	→*syn*	→TS	→*syn*
HF/STO-3G[b]	+21.61	+0.31	+21.55	+2.24	+21.10	+0.29	+21.53	−0.45	+20.12	+1.15	+21.84	+2.45
HF/3-21G[b]	+17.85	+0.32	+17.40	+2.18	+18.89	+0.48	+20.12	−0.58	+19.45	+1.56	+18.31	+1.73
HF/6-31+G*							+20.68	−0.13[b]				
B3LYP/6-31+G*							+14.46	−0.21				
HF/6-31+G*//HF/3-21G	+17.93	+0.08									+18.38	+1.88
HF/6-31+G*//HF/3-21G Onsager[c]	+17.87	−0.11									+18.30	+1.70
B3LYP/6-31+G*//HF/3-21G	+13.17	+0.14									+13.60	+1.75
Experimental ΔG[d]	+17.85	+0.35	+16.73	+1.24	+20.19	+0.67					+25.65	+0.56
Experimental ΔH	+17.33	−0.19	+16.15	+1.57	+20.52	+1.41					+25.05	+2.16

[a] Energies are relative to the respective *anti* conformers. [b] Zero-point energies are included. [c] The Onsager SCRF model is applied. [d] ΔG values calculated at 298 K.

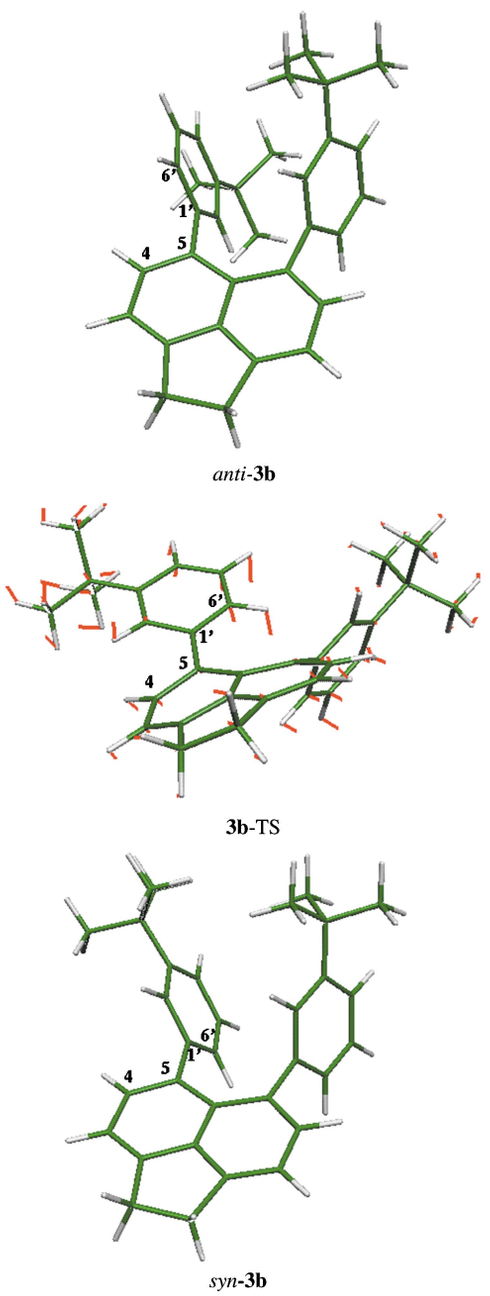

Fig. 2 Geometries along the *anti* to *syn* conversion pathway of **3b**, fully optimised at the HF/3-21G level of theory. The frequency arrows illustrate the imaginary frequency of **3b**-TS.

the experimental trend and is higher than for **2b** and **2c**. In the present study, the experimental activation barriers were determined by NMR in $CDCl_3$ (for **2b**, **2c**, and **2d**) or D_2O (for **3c**). Therefore, we tried to estimate the effect of solvent screening by performing Onsager SCRF calculations for compounds **2b** and **3c**. The resulting Onsager relative energies differ from the ones without solvent by less than 0.1 kcal mol^{-1}, indicating that the effect of modelling the solvent as a continuum of uniform relative permittivity is negligible. A noteworthy result is that density functional theory with the B3LYP functional underestimates the activation barriers by several kcal mol^{-1} for both molecules **2b** (single point calculation) and **3a** (full geometry optimisation). This is in contrast to studies on rotational barriers in heteroaromatic systems using density functionals with non-local corrections, where the DFT methods tended to overestimate the activation energy.[21,22] In these cases, however, no additional steric hindrance by an adjacent aromatic ring was involved. Finally, the relative energies of the *anti* and *syn* energy minima are only marginally affected by the level of theory.

When the activation energies are compared for **2b**, **2c**, **2d**, and **3c**, several trends are observed. Molecules **2b** and **2c** have very similar barriers for rotation. This can be explained by analysis of the corresponding transition state structures (see, for example, the transition state structure of **3b** in Fig. 2). It is the 2′-hydrogen on one aryl ring which has to "squeeze past" the other aryl ring, whereas the substituents in the 3′-position are not engaged in any repulsive interaction. For molecule **2d**, the methyl group in the 5′-position is forced to move past the other aryl ring during rotation. However, as there is much more space for a substituent in the *meta*-position (*i.e.* 3′/3″ and 5′/5″) compared to the *ortho*-position (*i.e.* 2′/2″ and 6′/6″), this leads to a moderate increase of the activation energy. In general the agreement between theory and experiment is very good, but for **3c** the calculations underestimated the rotational barrier by almost 7 kcal mol^{-1}. We therefore investigated the possibility of energetic lowering of the *syn*/*anti* atropisomers of **3c** through intramolecular hydrogen bonding between the OH groups. To this end geometry optimisations were performed up to the HF/6-31G** theoretical level on **3d**. Despite starting from different initial geometries, none of the optimisation runs converged to a minimum with a hydrogen bond or any similar intramolecular interaction. At the HF/6-31G** level the oxygen–oxygen distance was calculated to be 4.9 Å for this molecule. This value compares well with the oxygen–oxygen distances calculated for the *para*-methoxy substituted compounds (*i.e.* **2a**–**d** and **4c**). Evidently, the fact that the aryl rings are not parallel to one another results in a minimum oxygen–oxygen distance of approximately 5 Å, which is too large for intramolecular hydrogen bonding.

We proceeded to investigate the possibility of hydrogen bonding involving water molecules forming "bridges" between the two OH groups in **3c**. We inserted one or two water molecules between the OH groups and performed geometry optimisations on *anti*-**3c** at the HF/3-21G level of theory. The optimised geometries are displayed in Fig. 3. The **3c**–H_2O interaction energies calculated at the HF/6-31+G*//HF/3-21G level of theory are −5.52 for *anti*-**3c**·H_2O and −3.44 kcal mol^{-1} for and *anti*-**3c**·$2H_2O$, respectively, including corrections for the basis set superposition error. Interestingly, the calculations indicate that one water molecule stabilises the ground state of **3c** more than two water molecules. This can be explained by an analysis of the geometries of *anti*-**3c**·H_2O and *anti*-**3c**·$2H_2O$. In *anti*-**3c**·$2H_2O$ the two water molecules partially repel each other, and consequently the angles and distances of the hydrogen bonds are distorted. Also, the water molecules are pushed closer to the nearby *tert*-butyl groups, which leads to unfavourable interactions. In contrast, in *anti*-**3c**·H_2O the hydrogen bond geometry is not distorted and the water molecule is not involved in repulsive interactions. It appears that **3c** is set up ideally for accommodating one water molecule between its OH groups.

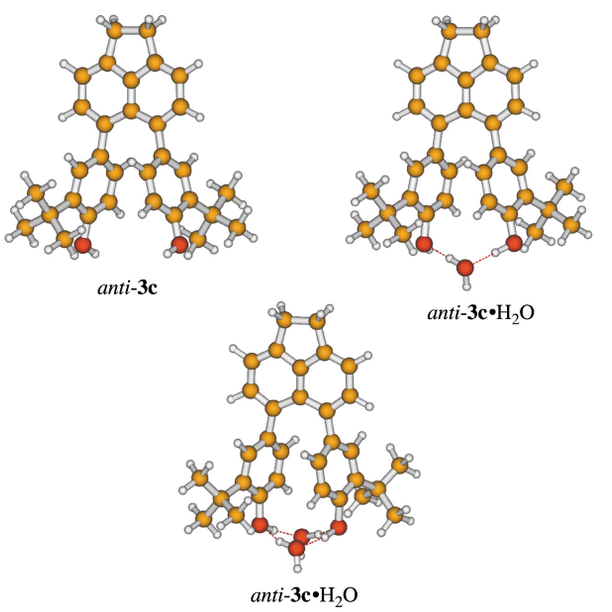

Fig. 3 Comparison of the HF/3-21G geometries of *anti*-**3c**, and *anti*-**3c** with one (*anti*-**3c**·H_2O) or two (*anti*-**3c**·$2H_2O$) water molecules. The dotted lines represent the hydrogen bonds between the water molecules and the OH groups of **3c**.

This is also indicated by the O–O distance, which decreases only slightly from 4.9 to 4.5 Å upon insertion of a water molecule. In the transition state of **3c**, the calculated O–O distance is increased to 7.1 Å, consequently leading to a destruction of the intramolecular hydrogen "bridge". Taking the stabilisation of *anti*-**3c** by 5.52 kcal mol^{-1} into account, the overall activation enthalpy required for rotation amounts to 23.90 (18.38 + 5.52) kcal mol^{-1}. This compares very well to the experimental value of 25.05 kcal mol^{-1}. Therefore, the increase in the activation barrier for **3c** as measured by NMR in DMSO–D_2O, can be explained largely through an intramolecular interaction, which exists only in the ground state and is mediated through a water molecule. It is also interesting to note that in the laboratory this compound is isolated as a monohydrate.[6a]

Single crystal X-ray crystallography

Different views of the single crystal X-ray structures of **2b**, **2c** and **2d** are given in Figs. 4 and 5 and associated data in Tables 1 and 3. It is interesting to note that in all three cases, crystals are isolated as single atropisomeric forms, *syn*-**2b**, *anti*-**2c** and *anti*-**2d**. This is perhaps a little surprising, and to our knowledge unique to this system, since theoretical (*vide supra*) and experimental studies (*vide infra*) clearly show that the difference in ground state energies of all three systems is very small. Since atropisomer interconversion occurs readily in solution one might expect a mixture of both atropisomeric forms in the solid state. We have previously observed the exclusive isolation of single atropisomeric crystals in these systems[5b] and therefore conclude that crystal packing forces must drive the formation of these single atropisomeric crystalline forms. The crystal structures are exactly as would be expected based on comparisons with previously reported structures[5b] and the ground state *ab initio* calculated structures. A series of selected interatomic distances, angles and torsional angles are given in Table 3, together with a comparison of their values with the appropriate *ab initio* structure. Five pieces of data are presented which can be used to describe the conformation of these molecules. The first two values, θ and ϕ, indicate the degree of distortion in these systems. As these values increase numerically, it indicates an increased degree of steric strain in the system; the angle θ is a measure of the in-plane distortion between the phenyl rings (where the plane refers to the acenaphthene scaffold), whilst the second value, ϕ, gives the out-of-plane distortion (Fig. 6). It should be noted that although ϕ is listed as having positive values, in all cases it can be clearly seen from Fig. 3 that these distortions are in opposite directions, *viz*. above and below the acenaphthene plane. Torsional angle τ_1 defines the conformation of the *peri*-phenyl

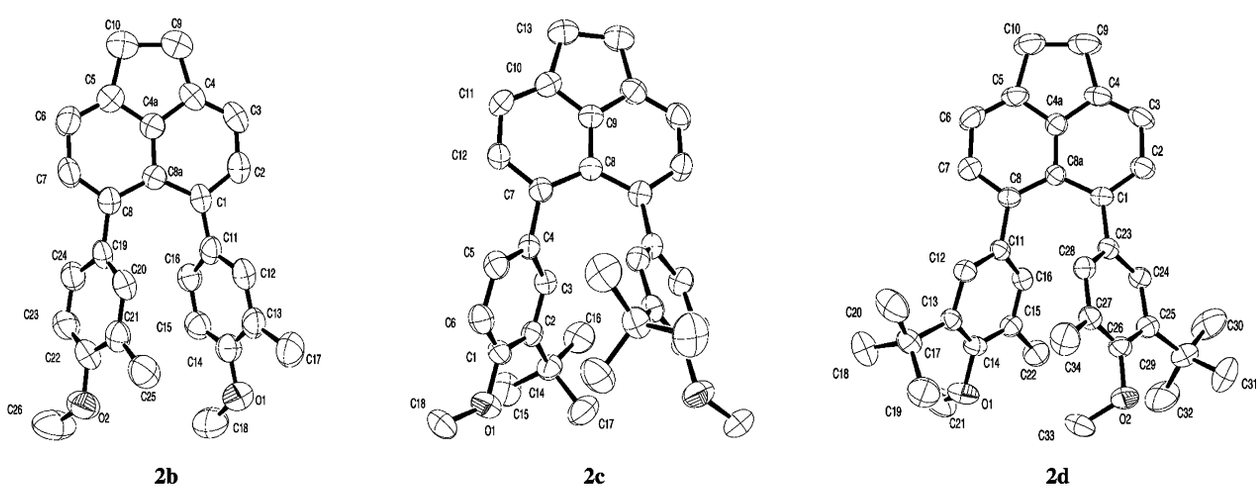

Fig. 4 ORTEP plots of **2b**–**d** (view 1) with hydrogen atoms omitted for clarity.

Table 3 Selected geometrical parameters for **2b–d**

Compound		θ/°	ϕ/°	τ_1/°	x/Å	O–O/Å
syn-**2b**	X-ray	24.78	0.56	60.2	3.151	4.445
			5.69	61.3		
	ab initio	25.01	1.15	67.2	3.101	4.929
			1.24	71.2		
anti-**2c**	X-ray	12.40	8.95[a]	124.0[a]	3.160	5.621
	ab initio	24.62	3.39[a]	113.6[a]	3.094	4.888
anti-**2d**	X-ray	23.29	10.66	125.2	3.095	4.935
			7.70	125.3		
	ab initio	24.98	10.83[a]	117.5[a]	3.146	5.984

[a] Only one value due to C_2 symmetry.

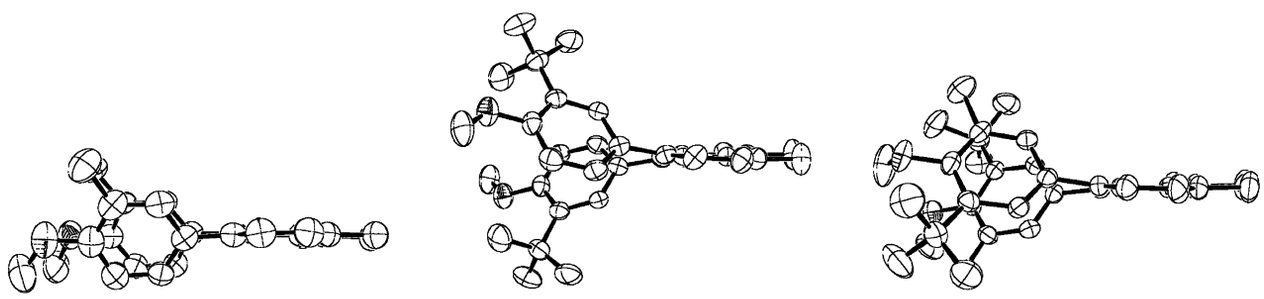

Fig. 5 ORTEP plots of **2b–d** (view 2) with hydrogen atoms omitted for clarity.

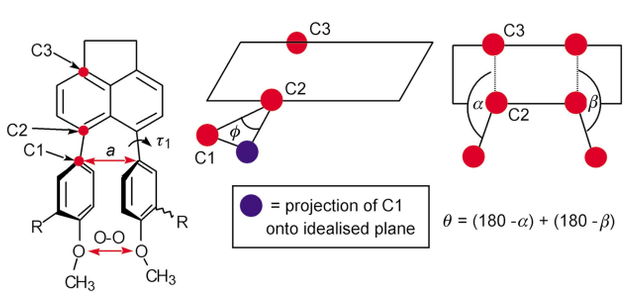

Fig. 6 Schematic representation of θ, ϕ, x and O–O for **2b–d**.

rings relative to the acenaphthene backbone, whilst x and O–O give straightforward interatomic distances.

The trends observed in θ and ϕ are broadly consistent with the increasing steric bulk in the molecules and in general there is also good agreement between experimental and theoretical data. The variations in ϕ are, as one might intuitively predict, based on the increase in steric bulk in the system, *viz.* **2b** < **2c** < **2d** for both experimental (**2b** $\phi_{average} = 3.13°$; **2c** $\phi = 8.95°$; **2d** $\phi_{average} = 9.18°$) and theoretical (**2b** $\phi_{average} = 1.20°$; **2c** $\phi = 3.39°$; **2d** $\phi = 10.83°$) values, with the largest discrepancy between experiment and theory being observed for **2c**. It is interesting to note that when the three structures are viewed along the axis which shows ϕ most clearly, cursory inspection appears to indicate that **2d** is actually more distorted than **2c** (Fig. 5). However, the values of ϕ show that this is clearly not the case. There is also good correlation between experiment and theory in the values of θ for **2b** and **2d**, but there is an obvious anomaly between the theoretical value for **2c** and the experimental value. This is readily rationalised by comparison with the changes in ϕ. When both angles are considered it is apparent that in the crystal system steric strain is relieved by employing a large distortion in ϕ of 8.95° for each *peri*-phenyl ring (*cf.* 3.39° for the theoretical value) whereas in the gas phase calculation steric strain is relieved through $\theta = 24.62°$ (*cf.* experimental 12.40° in **2c**). In summary, for **2b** the majority of steric strain is relieved through increasing θ for both experimental and theoretical situations; for **2c** there is an "either-or" situation, in which the majority of steric strain is relieved through one angle; finally in the most hindered system **2d**, both angles must distort to accommodate the increased steric bulk in the molecule.

The values of τ_1 show excellent agreement between experiment and theory and indicate that there is a clear need in all structures for the *peri*-phenyl rings to be staggered at an angle of approximately 60° to the acenaphthene backbone no matter what substituents are placed about the aryl rings. Within the series there is little variation in x (3.095–3.160 Å), which compares favourably with the range of values observed in the Cambridge Crystallographic Database (CCD) of 2.970–3.107 Å for related structures. The slight increase in x observed in this series of compounds when compared with those in the CCD can be easily rationalised by the increased steric strain in these systems. It should also be noted that when x is compared between related 5,6-acenaphthene and 1,8-naphthalene backbones in the CCD, there is a small but obvious increase of about 0.1 Å on moving from the 1,8-naphthalene backbone to the 5,6-acenaphthene backbone. Again this is entirely consistent with the molecular modelling results, which indicate that the presence of the benzylic bridge in acenaphthene results in an increased buckling of the acenaphthene ring, consequently increasing x. There is also excellent correlation between the values of x in the crystal structures and the *ab initio* calculations, with the largest variation between theory and experimental values of only 0.066 Å being observed in **2b**. Finally, it should be noted that there is considerable variation in O–O in the series **2b–2d** and also variation between experimental and theoretical values for each compound. This is not surprising, since O–O is effectively dependent on θ, ϕ and x.

NMR Structure and dynamics

The ^{1}H NMR spectrum of **2b**, measured at ambient temperature, showed considerable broadening for most of the resonances, but at lower temperature these resonances sharpened (see

Table 4 ^{1}H Chemical shifts for diaryl acenaphthenes **2b–d**

Compound	H3/H8 and H4/H7	H2′/H2″	H5′/H5″	H6′/H6″	H1/H2	Other signals
anti-**2b**	7.46–7.49	6.57	6.63	7.03	3.56	3.86 (–CH_3), 1.95 (–CH_3)
syn-**2b**	7.46–7.49	6.77	6.44	6.90	3.56	3.82 (–OCH_3), 2.07 (–CH_3)
anti-**2c**	7.44–7.53	6.85	6.61	7.02	3.55	3.78 (–OCH_3), 1.24 [–C(CH_3)$_3$]
syn-**2c**	7.44–7.53	7.04	6.57	6.96	3.55	3.80 (–OCH_3), 1.25 [–C(CH_3)$_3$]
anti-**2d**	7.48–7.55	6.82	7.08	—	3.57	3.77 (OCH_3), 1.29 [–C(CH_3)$_3$], 2.33 (–CH_3)
syn-**2d**	7.48–7.55	7.00	6.97	—	3.57	3.78 (OCH_3), 1.35 [–C(CH_3)$_3$], 2.25 (–CH_3)

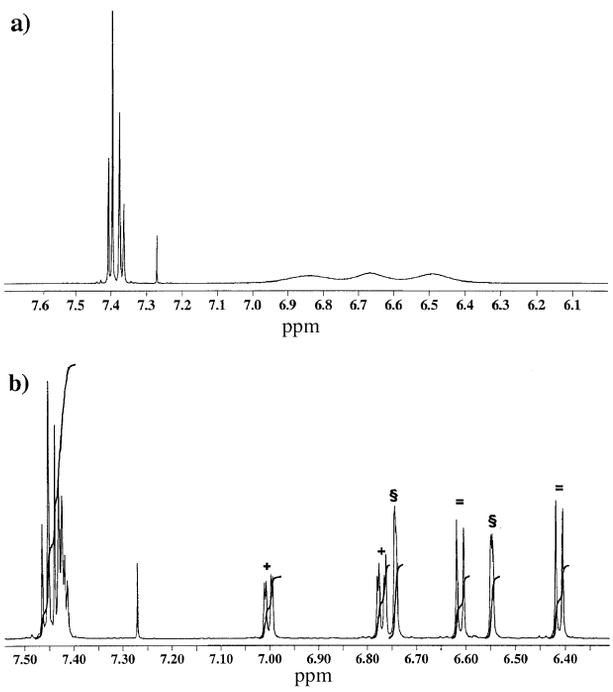

Fig. 7 High frequency (aromatic) region of the 600 MHz ^{1}H NMR spectrum of **2b** in $CDCl_3$ solution, a) measured at 323 K and b) measured at 243 K. The symbols, +, § and = indicate pairs of slowly exchanging resonances (see also Fig. 8).

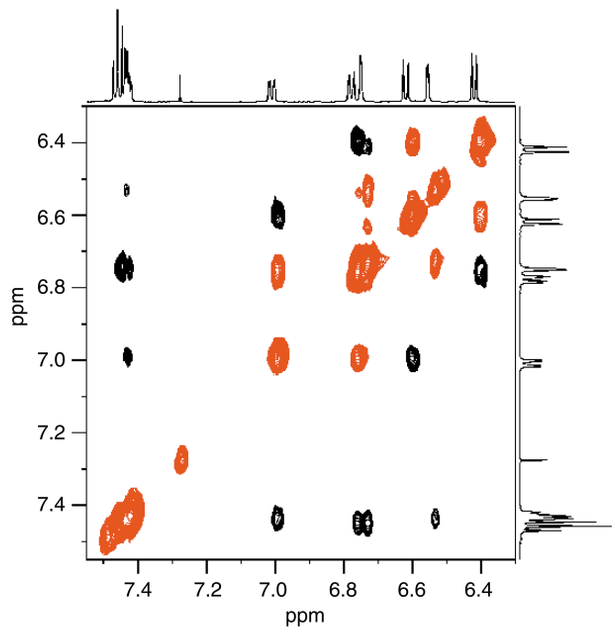

Fig. 8 High frequency (aromatic) region of the 600 MHz ^{1}H ROESY spectrum of **2b**, measured at 243 K with a mixing time of 400 ms. The off-diagonal peaks (black), which have the same phase as the diagonal peaks, correlate resonances in slow chemical exchange, and the off-diagonal peaks (red), with opposite phase to the diagonal, give NOE correlations.

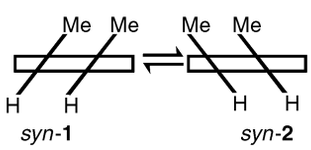

Fig. 9 Schematic representation of the degenerate conformers of the *syn*-atropisomer of **2b**, viewed from the mean plane of the acenaphthene moiety.

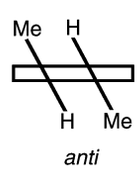

Fig. 10 Schematic representation of the *anti*-atropisomer of **2b**, viewed from the mean plane of the acenaphthene moiety.

spectrum at 243 K, Fig. 7). At the lower temperature the spectrum was consistent with the presence of two slowly interconverting atropisomers—the *syn* and the *anti* in near equal proportions. The ratio of the two atropisomers was measured by integration of the well-resolved ^{1}H resonances and varied between 1.24 at 213 K to 1.16 at 253 K. As described below, the atropisomer of **2b** in slight excess was assigned as *syn* on the basis of chemical shifts. Individual resonances were assigned as shown in Table 4 on the basis of chemical shift, couplings and integration, in addition to inter-proton Overhauser effects measured from the 2-dimensional ROESY spectra. A section of the high frequency region of the ROESY spectrum is shown in Fig. 8. Off-diagonal peaks, which are due to Overhauser effects, have opposite phase to the diagonal peaks. Off-diagonal peaks, which have the same phase as the diagonal, are due to (slow) chemical exchange between the *syn*- and *anti*-atropisomers, thus establishing correspondence between resonances in the two forms. In addition to those displayed in Fig. 8, other Overhauser effect correlations were observed to be consistent with the structures, *viz*. H3,8↔H1,2; H5′$_{syn}$↔OMe$_{syn}$; H5′$_{anti}$↔OMe$_{anti}$; H2′$_{syn}$↔3′Me$_{syn}$; H2′$_{anti}$↔3′Me$_{anti}$. There was also a weak correlation between the 3′Me$_{anti}$ resonance and the resonance for H5′$_{anti}$, which is probably an inter-ring effect. Fig. 9 shows the schematic *syn*-atropisomer of **2b** viewed from the mean plane of the acenaphthene moiety. For this atropisomer we must consider two equal energy conformers interconverting rapidly on the NMR time scale. It is this rapid equilibration which gives rise to the observed chemical shift equivalences. Fig. 10 shows the schematic *anti*-atropisomers of **2b** in the minimum energy conformation corresponding to that calculated above (also the conformation corresponding to that found in the X-ray analysis of *anti*-**2c** and *anti*-**2d**). The

calculated enthalpy difference between the *syn*- and *anti*-forms is small (less than 0.3 kcal mol^{-1}, see Table 2) with the *anti* being the more stable of the two. Because there are the two degenerate conformers possible for the *syn*-atropisomer and just one for the *anti*, the dynamic situation is best represented by Scheme 1.

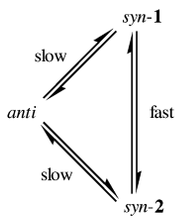

Scheme 1 Representation of the dynamic situation for **2b**.

An *assumed* value for $\Delta G^\circ = 250$ cal mol^{-1} at 243 K would give the ratio [*syn*-1 + *syn*-2]/[*anti*] about 1.2, which is approximately the same as the experimentally determined ratio (1.1_7). The temperature dependence of the putative ratio [total *syn*]/[*anti*] was used to derive the thermodynamic parameters ΔH° and ΔS° for the *anti*$\rightleftharpoons$*syn* − *i*, *i* = 1 or 2 equilibrium, and these were $\Delta H^\circ = -0.19$ kcal mol^{-1} and $\Delta S^\circ = -1.8$ cal K^{-1} mol^{-1}. This gives ΔG° at 243 K as 247 cal mol^{-1} in favour of the *anti*-form; however because the *syn* exists in two degenerate conformations, the total proportion of *syn* exceeds the *anti*.

In the temperature range 273 to 323 K the ^{1}H resonances broaden and coalesce, and the rate coefficient, *k* for the process *anti* to *syn* was determined by iterative fitting of the resonances due to the 3′Me groups. The rate coefficient varied in the range 2.4 s^{-1} at 273 K to 452 s^{-1} at 323 K, and plots of ln (*k*) *vs.* T^{-1} (Arrhenius) and ln (*k*/*T*) *vs.* T^{-1} (Eyring) were both linear. The former plot yielded a value for the Arrhenius activation energy, $E_a = 17.9$ kcal mol^{-1}, and the Arrhenius A-factor, $A = 5.4 \times 10^{14}$. The Eyring plot yielded a value for the activation enthalpy, $\Delta H^\ddagger = 17.3$ kcal mol^{-1} and activation entropy, $\Delta S^\ddagger = 7.1$ cal K^{-1} mol^{-1}.

The ^{1}H NMR spectrum of **2c** at ambient temperature showed broadening of the resonances, which sharpened at lower temperature. In the temperature range 250 to 280 K the well resolved resonances due to the *syn*- and *anti*-atropisomers were observed. The ratio of the two sets of resonances, determined by integration, varied in the range 0.07 at 250 K to 0.11 at 290 K, and the major component was assigned as the *anti*-atropisomer. This assignment is consistent with the calculated greater stability of the *anti*-atropisomer (Table 2). The resonances were assigned by consideration of chemical shifts, couplings, integration and inter-proton Overhauser and exchange effects observed in ROESY spectra, and these assignments are given in Table 4. It is noteworthy that the change in phenyl ring proton chemical shifts on passing from the *anti*- to the *syn*-form is entirely consistent with the dimethyl compound **2b**, *i.e.* H2′ shifts to higher frequency while H5′ and H6′ both shift to lower frequency (Table 4). The [*syn*] : [*anti*] ratio data as a function of temperature were used to derive the thermodynamic parameters $\Delta H^\circ = 1.57$ kcal mol^{-1} and $\Delta S^\circ = 1.13$ cal K^{-1} mol^{-1}. In the temperature range 280 to 330 K the resonances broadened and coalesced and iterative fitting of the band shapes gave the *anti* to *syn* exchange range coefficients, *k*, which varied in the range 2.6 s^{-1} at 290 K to 84.6 s^{-1} at 330 K. As for **2b** (above) the Arrhenius and Eyring plots were both linear and gave values for the Arrhenius activation energy, $E_a = 16.7$ kcal mol^{-1} and A-factor, $A = 1.1 \times 10^{13}$, and the Eyring parameters, $\Delta H^\ddagger = 16.15$ kcal mol^{-1} and $\Delta S^\ddagger = -0.9$ cal K^{-1} mol^{-1}.

The ^{1}H NMR spectra of **2d** again showed two sets of resonances at lower temperature (down to 203 K) which coalesced at the higher temperature (343 K). The ratio of the two sets of resonances, determined by integration varied in the range 0.10 at 203 K to 0.21 at 253 K, and the major set of resonances was assigned to the *anti*-atropisomer, to be consistent with the greater demand of the *tert*-butyl group over the methyl group for the *anti*-arrangement (**2c** *cf.* **2b**). The resonances were assigned as described above (see Table 4), and the lower temperature [*syn*]/[*anti*] ratio data gave $\Delta H^\circ = 1.41$ kcal mol^{-1} and $\Delta S^\circ = 2.4$ cal K^{-1} mol^{-1}. The higher temperature kinetic data gave values for the Arrhenius activation energy, $E_a = 20.2$ kcal mol^{-1} and A-factor, $A = 4.3 \times 10^{15}$, and the Eyring parameters, $\Delta H^\ddagger = 20.5$ kcal mol^{-1} and $\Delta S^\ddagger = 13.9$ cal K^{-1} mol^{-1}.

^{1}H NMR spectra of the di-*tert*-butyl phenol **3c** at ambient temperature showed broadening of the resonances due to exchange between the *syn*- and *anti*-atropisomers, in both acetone and chloroform solutions, but in order to achieve coalescence a higher boiling solvent was necessary and the cryoprotective mixture[23] of DMSO–water was selected (see Methods section) which allowed measurements at both low and high temperatures. Chemical shift assignments were made using the experiments described above (see Table 4). The [*syn*] : [*anti*] ratio varied in the range 0.16 at 243 K to 0.27 at 273 K and gave $\Delta H^\circ = 2.16$ kcal mol^{-1} and $\Delta S^\circ = 5.4$ cal K^{-1} mol^{-1}. The higher temperature kinetic data gave values for the Arrhenius activation energy, $E_a = 25.7$ kcal mol^{-1} and *A*-factor, $A = 1.6 \times 10^{19}$, and the Eyring parameters, $\Delta H^\ddagger = 25.1$ kcal mol^{-1} and $\Delta S^\ddagger = 27.3$ cal K^{-1} mol^{-1}.

Conclusions

This class of molecules has been the topic of investigation for more than 30 years, due to their potential application as chiral auxiliaries and the inherent challenge that their synthesis and dynamics present. Many attempts have been made to prevent atropisomer interconversion through different substitution patterns to probe steric and electronic effects, but to no avail. Through a combination of different experimental and theoretical techniques, the present investigation was able to establish a fundamental understanding of the process of atropisomer interconversion.

It appears that calculations at the HF/3-21G level of theory already give good agreement with experimental activation barriers, which makes systems of this size computationally tractable. The validity of the calculations is strongly supported by comparsion with both single crystal X-ray structure analysis (of **2b**, **2c**, and **2d**) and NMR spectroscopic techniques to measure the barrier height for rotation. The DFT-B3LYP method, as well as semi-empirical calculations, appear to underestimate the activation energies.

Although the energy differences between the *syn*- and *anti*-atropisomers are relatively small, as indicated by the calculations and NMR studies, in the crystal structures only one atropisomer is found: **2b** crystallises as *syn*, whereas for **2c** and **2d** only the *anti*-forms are observed. This could be due to crystal packing effects, but it also correlates very well with the distribution of the major atropisomers in solution found by NMR. Since the major solution form is observed in the solid state we speculate that as the dominant solution form starts to crystallize, the *anti*–*syn* equilibrium is disturbed and the minor form is converted into the dominant form in order to re-establish the solution equilibrium. Taking this to an extreme would eventually result in the isolation of a single atropisomeric species.

Instrumental to the analysis has been the calculation of the transition state structures for rotation. These structures indicate a remarkable flexibility of the acenaphthene ring system and reveal that bulky substituents in the *meta*-positions (*i.e.* 3′/3″ and 5′/5″) are not capable of stabilising a single atropisomeric form. It therefore seems that additional chemistry has to be applied in order to stabilise the atropisomers. Preliminary calculations in this area have revealed that certain substituents

in positions 4 and 7 of an acenaphthene or 2 and 7 of a naphthalene scaffold might provide enough steric hindrance to prevent atropisomer interconversion. We are currently engaged in a synthetic programme in order to test this hypothesis and will report the results of these studies shortly.

Acknowledgements

We thank the EPSRC for studentships (to MS, GR/97311210 and RN, GR/98700139) and Dr H. Toms and Mr P. Haycock of the University of London Inter Collegiate Research Service (ULIRS) for their assistance in measuring NMR spectra with the BRUKER AMX-600. We also wish to acknowledge the use of the EPSRC's Chemical Database Service at Daresbury.[24]

References

1 (*a*) H. O. House, R. W. Magin and H. W. Thompson, *J. Org. Chem.*, 1963, **28**, 2403; (*b*) H. O. House and R. W. Bashe, *J. Org. Chem.*, 1965, **30**, 2942; (*c*) H. O. House and R. W. Bashe, *J. Org. Chem.*, 1967, **32**, 784; (*d*) H. O. House, W. J. Campbell and M. Gil, *J. Org. Chem.*, 1970, **35**, 1815; (*e*) H. O. House, D. G. Koepsell and W. J. Campbell, *J. Org. Chem.*, 1972, **37**, 1003.

2 (*a*) J. Seyden-Penne, *Chiral Auxiliaries and Ligands in Asymmetric Synthesis*, Wiley, New York, 1995; (*b*) J. K. Whitesell, *Chem. Rev.*, 1989, **89**, 1581.

3 (*a*) R. L. Clough and J. D. Roberts, *J. Am. Chem. Soc.*, 1976, **98**, 1018; (*b*) P. Wahl, C. Krieger, D. Schweitzer and H. A. Staab, *Chem. Ber.*, 1984, **117**, 260.

4 (*a*) R. Cosmo and S. Sternhell, *Aust. J. Chem.*, 1987, **40**, 1107; (*b*) F. Cozzi, M. Cinquini, R. Annunziata, T. Dwyer and J. S. Siegel, *J. Am. Chem. Soc.*, 1992, **114**, 5729; (*c*) F. Cozzi, M. Cinquini, R. Annunziata, T. Dwyer and J. S. Siegel, *J. Am. Chem. Soc.*, 1993, **115**, 5330; (*d*) F. Cozzi, F. Ponzini, R. Annunziata, M. Cinquini and J. S. Siegel, *Angew. Chem., Int. Ed. Engl.*, 1995, **34**, 1019.

5 (*a*) M. Watkinson, A. Whiting and C. A. McAuliffe, *J. Chem. Soc., Chem. Commun.*, 1994, 2141; (*b*) B. Beagley, N. C. Edge, N. Jaiboon, J. J. James, C. A. McAuliffe, M. S. Thorpe, M. Watkinson, A. Whiting and D. C. Wright, *Tetrahedron*, 1996, **52**, 10193.

6 (*a*) M. Steele, M. Watkinson and A. Whiting, *J. Chem. Soc., Perkin Trans. 1*, 2001 (DOI: 10.1039/b008319o); (*b*) M. Steele, M. Watkinson and A. Whiting, *Tetrahedron Lett.*, 2000, **41**, 6915.

7 J. A. Zoltewicz, N. M. Maiar and W. M. F. Fabian, *J. Org. Chem.*, 1997, **62**, 3215.

8 F. Cozzi and J. S. Siegel, *Pure Appl. Chem.*, 1995, **67**, 683.

9 Y. Nagawa, K. Honda and H. Nakanishi, *Magn. Reson. Chem.*, 1996, **34**, 78.

10 Gaussian 98, Revision A.7, M. J. Frisch, G. W. Trucks, H. B. Schlegel, G. E. Scuseria, M. A. Robb, J. R. Cheeseman, V. G. Zakrzewski, J. A. Montgomery Jr., R. E. Stratmann, J. C. Burant, S. Dapprich, J. M. Millam, A. D. Daniels, K. N. Kudin, M. C. Strain, O. Farkas, J. Tomasi, V. Barone, M. Cossi, R. Cammi, B. Mennucci, C. Pomelli, C. Adamo, S. Clifford, J. Ochterski, G. A. Petersson, P. Y. Ayala, Q. Cui, K. Morokuma, D. K. Malick, A. D. Rabuck, K. Raghavachari, J. B. Foresman, J. Cioslowski, J. V. Ortiz, A. G. Baboul, B. B. Stefanov, G. Liu, A. Liashenko, P. Piskorz, I. Komaromi, R. Gomperts, R. L. Martin, D. J. Fox, T. Keith, M. A. Al-Laham, C. Y. Peng, A. Nanayakkara, C. Gonzalez, M. Challacombe, P. M. W. Gill, B. Johnson, W. Chen, M. W. Wong, J. L. Andres, M. Head-Gordon, E. S. Replogle and J. A. Pople, Gaussian, Inc., Pittsburgh PA, 1998.

11 M. J. S. Dewar, E. G. Zoebisch and E. F. Healy, *J. Am. Chem. Soc.*, 1985, **107**, 3902.

12 J. B. Collins, P. V. R. Schleyer, J. S. Binkley and J. A. Pople, *J. Chem. Phys.*, 1976, **64**, 5142.

13 J. S. Binkley, J. A. Pople and W. J. Hehre, *J. Am. Chem. Soc.*, 1980, **102**, 939.

14 P. C. Hariharan and J. A. Pople, *Theor. Chim. Acta*, 1973, **28**, 213.

15 A. D. Becke, *J. Chem. Phys.*, 1993, **98**, 5648.

16 T. Clark, J. Chandrasekhar, G. W. Spitznagel and P. V. R. Schleyer, *J. Comput. Chem.*, 1983, **4**, 29.

17 M. W. Wong, M. J. Frisch and K. B. Wiberg, *J. Am. Chem. Soc.*, 1991, **113**, 4776.

18 SHELX97 [Includes SHELXS97, SHELXL97, CIFTAB]—Programs for Crystal Structure Analysis (Release 97–2), G. M. Sheldrick, Institüt für Anorganische Chemie der Universität, Tammanstrasse 4, D-3400 Göttingen, Germany, 1998.

19 For a discussion of the conditions under which motional nulling of the ^{1}H–^{1}H NOE occurs, see D. Neuhaus and M. P. Williamson, *The Nuclear Overhauser Effect in Conformational Analysis*, VCH, New York, 1989, p. 36.

20 T. Lenzen and G. Hagele, WIN-DYNA 32, version 1.01, release 981101, Bruker Analytik GmbH, 1994–1998.

21 P. M. Viruela, R. Viruela and E. Orti, *Int. J. Quantum Chem.*, 1998, **70**, 303.

22 M. Viruela, R. Viruela, E. Orti and J. L. Bredas, *J. Am. Chem. Soc.*, 1997, **119**, 1360.

23 (*a*) P. Douzou and G. A. Petsko, *Adv. Protein Chem.*, 1984, **36**, 245; (*b*) A. Motta, D. Picone, T. Tancredi and P. A. Temussi, *Tetrahedron*, 1988, **44**, 975.

24 (*a*) D. A. Fletcher, R. F. McMeeking and D. Parkin, *J. Chem. Inf. Comput. Sci.*, 1996, **36**, 746; (*b*) F. H. Allen and O. Kennard, *Chem. Des. Automat. News*, 1993, **8**, 1; F. H. Allen and O. Kennard, *Chem. Des. Automat. News*, 1993, **8**, 31.